Heterogeneous Track-to-Track Fusion

TING YUAN
YAAKOV BAR-SHALOM
XIN TIAN

Track-to-track fusion using estimates from multiple sensors can achieve better estimation performance than single sensor tracking. If the local sensors use different system models in different state spaces, the problem of heterogeneous track-to-track fusion arises. Compared with homogeneous track-to-track fusion that assumes the same system model for different sensors, the heterogeneous case poses two major challenges. The first one is that we have to fuse estimates from different state spaces (related by a certain nonlinear transformation). The second is the estimation errors' dependence problem, which is generally recognized as the "common process noise effect." Different heterogeneous track-to-track fusion approaches, namely, the linear minimum mean square error approach and the maximum likelihood approach, are presented and compared with the corresponding centralized measurement tracker/fuser (also known as measurement-to-track fuser).

Manuscript submitted on February 24, 2011; revised June 20, 2011; released for publication July 13, 2011.

Refereeing of this contribution was handled by Dr. Peter K. Willett.

Authors' address: University of Connecticut, ECE Department, 371 Fairfield Way, Unit 2157, Storrs, CT 06279, E-mail: ({tintti, ybs, xin.tian}@engr.uconn.edu).

1. INTRODUCTION

In a multisensor tracking system, the best target state estimation performance is obtained by a centralized tracker/fuser (CTF), by directly sending to the fusion center (FC) all the measurements of the local sensors.[1] However, in many practical situations, because of communication constraints, each local sensor has its own information processing system and sends only tracks to the FC, which appropriately fuses tracks from different local sensors to achieve comparable estimation performance to that of the CTF [3].

For track-to-track fusion (T2TF) from homogeneous local trackers (which use the same target state space), the "common process noise effect" (quantified by the crosscovariance matrix) has been theoretically well-established [3]. However, there is no known way for the calculation of the crosscovariance matrix in the case of heterogeneous local trackers (which use the different target state spaces). The difficulty to evaluate the crosscovariance matrix in the heterogeneous case is that it requires to capture the "common" part of process noises from different state spaces to quantify the crosscorrelation.

In the literature there are few works dealing with the model heterogeneity. A heterogeneous T2TF fusion approach was presented in [6] to fuse the tracks from an active sensor and a passive sensor with different state vectors. However, the fusion was done by using the full Cartesian state estimates (from an active sensor) to update the smaller angular state estimates (from a passive sensor). An expression for the steady state crosscovariance matrix for dissimilar sensors (of the same state vector but with different measurement noise variances) employing α-β filters was derived in [9]. For this specified case, a condition to guarantee the positivity of crosscovariance matrix was presented, which does not always hold in the heterogeneous case.

The goal of this paper is to fuse the tracks from heterogeneous local sensors (an active and a passive one) with different state spaces to yield fused estimates in the full state space and evaluate the performance of the resulting heterogeneous T2TF. The fusion configuration considered is the one without memory at the FC and no feedback to the local sensors (T2TFwoMnf in the terminology of [10]).

In view of the fact that there is no known way to evaluate the crosscovariance of the estimation errors in the case of heterogeneous sensors, a Monte Carlo (MC) investigation of these errors' crosscorrelations is carried out.

The paper is organized as follows. Section 2 formulates the heterogenous T2TF problem. Two approaches, namely, the linear minimum mean square error (LMMSE) and maximum likelihood (ML) heterogeneous T2TF are presented in Section 3. The cross-

[1]The superiority of CTF over other configurations can be proved only for the linear case [3].

correlation analysis by MC simulations is presented in Section 4. Section 5 evaluates the proposed approaches in a tracking scenario with an active sensor and a passive sensor. Section 6 provides conclusions.

2. THE HETEROGENOUS TRACK-TO-TRACK FUSION PROBLEM

Without loss of generality, consider the following state-space models

$$\mathbf{x}^i(k+1) = f^i(\mathbf{x}^i(k)) + \mathbf{v}^i(k) \tag{1}$$

$$\mathbf{z}^i(k) = h^i(\mathbf{x}^i(k)) + \mathbf{w}^i(k) \tag{2}$$

at sensor i and

$$\mathbf{x}^j(k+1) = f^j(\mathbf{x}^j(k)) + \mathbf{v}^j(k) \tag{3}$$

$$\mathbf{z}^j(k) = h^j(\mathbf{x}^j(k)) + \mathbf{w}^j(k) \tag{4}$$

at sensor j. In the above, $f^s[\cdot]$ and $h^s[\cdot]$, $s = i, j$, are different and can be nonlinear; $\mathbf{v}^s(\cdot)$ and $\mathbf{w}^s(\cdot)$, $s = i, j$, are the process and measurement noises, respectively.

Further, note that $\mathbf{x}^i$ and $\mathbf{x}^j$ are in different state spaces. Let $\mathbf{x}^i$ be the larger dimension state (e.g., full Cartesian position and velocity in two-dimensional space for tracking with an active sensor)

$$\mathbf{x}^i = [x \quad \dot{x} \quad y \quad \dot{y}]' \tag{5}$$

and $\mathbf{x}^j$ be the smaller dimension state (e.g., angular position and velocity for tracking with a passive sensor)

$$\mathbf{x}^j = [\theta \quad \dot{\theta}]'. \tag{6}$$

These state vectors have the nonlinear relationship

$$\mathbf{x}^j \triangleq g(\mathbf{x}^i). \tag{7}$$

The two sensors are assumed synchronized[2] and the time index k for sampling time t_k will be omitted if there is no ambiguity.

The corresponding estimates (approximate conditional means) at these heterogeneous local sensors are $\hat{\mathbf{x}}^i$ with (conditional) covariance matrix

$$P^i \triangleq E[(\mathbf{x}^i - \hat{\mathbf{x}}^i)(\mathbf{x}^i - \hat{\mathbf{x}}^i)'] \tag{8}$$

and $\hat{\mathbf{x}}^j$ with (conditional) covariance matrix

$$P^j \triangleq E[(\mathbf{x}^j - \hat{\mathbf{x}}^j)(\mathbf{x}^j - \hat{\mathbf{x}}^j)']. \tag{9}$$

The problem is how to carry out the fusion of the estimate $\hat{\mathbf{x}}^i$ with P^i and the estimate $\hat{\mathbf{x}}^j$ with P^j to achieve a better estimation performance for the full state of interest $\mathbf{x}^i$.

[2]Generalization to asynchronous sensors is possible [11], but the notations become very cumbersome. Without considering the crosscovariance matrix, the extension to asynchronous case is straightforward. If the crosscovariance matrix is considered (for the configuration with no memory at the FC and no information feedback to the local trackers), each track's latest estimate available at the FC is predicted to the fusion time and then they are fused using the corresponding covariance matrices.

3. THE HETEROGENOUS TRACK-TO-TRACK FUSION

To illustrate the effect of the crosscovariance, consider the simple homogeneous T2TF in the linear-Gaussian and symmetric case with the local track covariance matrices $P_S^1 = P_S^2 = P_S$ and the crosscovariance matrices $P_S^{12} = P_S^{21} = P_S^X$. The resulting fused estimate and its covariance matrix are [3]

$$\hat{\mathbf{x}}_S^F = \tfrac{1}{2}(\hat{\mathbf{x}}_S^1 + \hat{\mathbf{x}}_S^2) \tag{10}$$

$$P_S^F = P_S^1 - (P_S^2 - P_S^{12})(P_S^1 + P_S^2 - P_S^{12} - P_S^{21})(P_S^1 - P_S^{21}) \tag{11}$$

$$= \tfrac{1}{2}P_S + \tfrac{1}{2}P_S^X. \tag{12}$$

In this case, the fused estimate $\hat{\mathbf{x}}_S^F$ in (10) is independent of the crosscovariance because of the assumed symmetry. However, the corresponding covariance P_S^F in (11) has a term that depends on the crosscovariance. If $P_S^X > 0$, the fusion is optimistic if one ignores the crosscovariance (in which case the fuser calculated covariance is $\frac{1}{2}P_S$, i.e., smaller than what it should be); if $P_S^X < 0$, the fusion is pessimistic.

The crosscovariance for homogeneous fusion follows from a Lyapunov equation [3] and, consequently, it is always positive semi-definite. In the heterogeneous case while there is no known way to compute the crosscovariance matrix, shown in Appendix C using MC simulations, some of the crosscorrelations are positive and some are negative. They depend on the relative geometry of the two sensors and the target, as well as the target maneuvers. To further complicate the situation, the maneuvers are unknown deterministic, rather than (zero-mean white) process noise and the crosscovariance based on the process noise can be substantially different from what the maneuver causes.

The following subsections present two fusers that assume the crosscovariance is available.

3.1. The LMMSE Fuser

The first approach to heterogeneous T2TF is to use the linear technique based on the fundamental equations of LMMSE estimation [2]. Considering the full state estimate $\hat{\mathbf{x}}^i$ as the prediction and the smaller state estimate $\hat{\mathbf{x}}^j$ as the measurement, we have the LMMSE fused estimate

$$\hat{\mathbf{x}}^i_{\text{LMMSE}} = \hat{\mathbf{x}}^i + P_{\mathbf{xz}}P_{\mathbf{zz}}^{-1}[\hat{\mathbf{x}}^j - g(\hat{\mathbf{x}}^i)] \tag{13}$$

with the corresponding fused covariance matrix

$$P^i_{\text{LMMSE}} = P^i - P_{\mathbf{xz}}P_{\mathbf{zz}}^{-1}P_{\mathbf{xz}}' \tag{14}$$

where (as the details shown in Appendix A)

$$P_{\mathbf{xz}} \triangleq E[(\mathbf{x}^i - \hat{\mathbf{x}}^i)(\hat{\mathbf{x}}^j - g(\hat{\mathbf{x}}^i))'] \approx P^i(G^i)' - P^{ij} \tag{15}$$

$$P_{\mathbf{zz}} \triangleq E[(\hat{\mathbf{x}}^j - g(\hat{\mathbf{x}}^i))(\hat{\mathbf{x}}^j - g(\hat{\mathbf{x}}^i))'] \approx P^j - G^iP^{ij} - P^{ji}(G^i)' + G^iP^i(G^i)' \tag{16}$$

with G^i the Jacobian of $g(\mathbf{x}^i)$

$$G^i \triangleq [\nabla_{\mathbf{x}^i} g(\mathbf{x}^i)']'_{\mathbf{x}^i=\hat{\mathbf{x}}^i} \tag{17}$$

and P^{ij} the crosscovariance matrix

$$P^{ij} \triangleq E[(\mathbf{x}^i - \hat{\mathbf{x}}^i)(\mathbf{x}^j - \hat{\mathbf{x}}^j)']. \tag{18}$$

3.2. The ML Fuser

Under the Gaussian assumption, the heterogeneous T2TF problem can be solved by minimizing the negative log-likelihood function[3]

$$\begin{aligned} L &= -\ln p(\hat{\mathbf{x}}^i, \hat{\mathbf{x}}^j | \mathbf{x}^i) \\ &\propto \left(\begin{bmatrix} \hat{\mathbf{x}}^i \\ \hat{\mathbf{x}}^j \end{bmatrix} - \begin{bmatrix} \mathbf{x}^i \\ \mathbf{x}^j \end{bmatrix} \right)' P^{-1} \left(\begin{bmatrix} \hat{\mathbf{x}}^i \\ \hat{\mathbf{x}}^j \end{bmatrix} - \begin{bmatrix} \mathbf{x}^i \\ \mathbf{x}^j \end{bmatrix} \right) \end{aligned} \tag{19}$$

where (7) has been used and

$$P = \begin{bmatrix} P^i & P^{ij} \\ P^{ji} & P^j \end{bmatrix}. \tag{20}$$

Then the ML fused estimate is the solution of

$$\nabla_{\mathbf{x}^i} L = 0. \tag{21}$$

Because of the nonlinearity of the function $g(\mathbf{x}^i)$, there is no explicit expression for the solution of (21). It can be solved by a numerical search, e.g., the gradient projection algorithm. The result is denoted as $\hat{\mathbf{x}}^i_{\mathrm{ML}}$ and the corresponding covariance matrix is

$$P^i_{\mathrm{ML}} = \left([I \quad G^i] P^{-1} \begin{bmatrix} I \\ G^i \end{bmatrix} \right)^{-1} \tag{22}$$

where G^i is defined in (17) and I is the identity matrix (4×4 in our case).

The results of $\hat{\mathbf{x}}^i_{\mathrm{LMMSE}}$ with P^i_{LMMSE} and $\hat{\mathbf{x}}^i_{\mathrm{ML}}$ with P^i_{ML} will be examined and compared with the CTF which processes all the measurements (from both the active and the passive sensor) in the FC in the simulation section.

4. THE CROSSCORRELATION IN HETEROGENEOUS FUSION

It has been recognized that, although different local sensors typically have independent measurement noises, the process noises for the motion models at these sensors belong to the same target and, consequently, will lead to (cross)correlated state estimation errors. This is the so-called "common process noise effect" [3]. For the heterogenous case, the common process noise effect, as it is embedded into the estimates from different sensors for the same target, also exists. However, since the estimates are in different state spaces, there is no known way to capture the "common" part exactly.

The dependence of the estimation errors can be quantified by the crosscovariance matrix, and the more accurately the crosscovariance matrix is obtained, the better the heterogeneous track-to-track fusion performance will be. However, the difference between the motion models for different sensors prohibits the evaluation of the crosscovariance matrix by the exact method described in [3] (limited to the homogeneous case and linear systems). Even this exact method is not considered practical since it requires information that is typically not available at the FC (the local filter gains).

While process noise is used in the motion equations to model the target maneuvers,[4] these maneuvers are, however, not stochastic processes. Consequently, MC simulations will be used to evaluate the crosscorrelation of the estimation errors from different sensors. As shown in Appendix C, considering the estimates from different local sensors in each MC run as one sample and evaluating the sample crosscorrelation coefficients, we observe both negative and positive crosscorrelations of the estimation errors from the heterogeneous local sensors in different parts of the target trajectory.

The fact that these crosscorrelations can be, unlike in the linear homogeneous case (when they are always positive), sometimes positive and sometimes negative is shown as follows. According to (14), the information matrix (assuming P^{ij} is available) is

$$\begin{aligned} J &= (P^F)^{-1} \\ &= [P^i - [P^i(G^i)' - P^{ij}][P^j - G^i P^{ij} - P^{ji}(G^i)' + G^i P^i (G^i)']^{-1} \\ &\quad \times [P^i(G^i)' - P^{ij}]']^{-1} \\ &\triangleq [P^i - [P^i(G^i)' - P^{ij}][P^j + G^i P^i (G^i)' + U]^{-1} \\ &\quad \times [P^i(G^i)' - P^{ij}]']^{-1} \end{aligned} \tag{23}$$

where

$$U \triangleq -G^i P^{ij} - P^{ji}(G^i)'. \tag{24}$$

Assuming $P^{ij} = 0$ (its elements are all zero), designated as the "uncorrelated" assumption (denoted concisely as "uncorr"), then (23) can be simplified (by the matrix inversion lemma) as

$$\begin{aligned} J(P^{ij} = 0) &= [P^i - P^i(G^i)'[P^j + G^i P^i (G^i)']^{-1} G^i (P^i)']^{-1} \\ &= (P^i)^{-1} - [(P^i)^{-1} P^i (G^i)'] \\ &\quad \times [G^i (P^i)' (P^i)^{-1} P^i (G^i)' - P^j - G^i P^i (G^i)']^{-1} \\ &\quad \times [(P^i)^{-1} P^i (G^i)']' \\ &= (P^i)^{-1} + (G^i)'(P^j)^{-1} G^i. \end{aligned} \tag{25}$$

[3] As it is pointed out in [4], the LMMSE T2TF approach is, in the linear Gaussian case, optimal in ML sense.

[4] The whiteness is necessary so the state is a Markov process, a sine qua non prerequisite for any recursive estimation algorithm [2].

If $P^{ij} \neq 0$ (this is denoted as "corr" for conciseness), then we have

$$\begin{aligned} J(P^{ij} \neq 0) &= (P^i)^{-1} - [(G^i)' - (P^i)^{-1}P^{ij}] \\ &\quad \cdot [[P^i(G^i)' - P^{ij}]'(P^i)^{-1}[P^i(G^i)' - P^{ij}] \\ &\quad - [P^j + G^iP^i(G^i)' + U]]^{-1} \\ &\quad \cdot [(G^i)' - (P^i)^{-1}P^{ij}]' \\ &\triangleq (P^i)^{-1} + [(G^i)' - (P^i)^{-1}P^{ij}] \\ &\quad \cdot [P^j + W]^{-1}[(G^i)' - (P^i)^{-1}P^{ij}]' \end{aligned} \tag{26}$$

where

$$\begin{aligned} W &\triangleq [G^iP^i(G^i)' + U] - [P^i(G^i)' - P^{ij}]'(P^i)^{-1}[P^i(G^i)' - P^{ij}] \\ &= -P^{ji}(P^i)^{-1}P^{ij}. \end{aligned} \tag{27}$$

Equation (26) can be written as (the generic matrix inversion lemma is used)

$$\begin{aligned} J(P^{ij} \neq 0) &= (P^i)^{-1} + [(G^i)' - (P^i)^{-1}P^{ij}] \\ &\quad \cdot [(P^j)^{-1} - (P^j)^{-1}W(P^j)^{-1}[I + W(P^j)^{-1}]^{-1}] \\ &\quad \cdot [(G^i)' - (P^i)^{-1}P^{ij}]' \\ &\triangleq (P^i)^{-1} + [(G^i)' - (P^i)^{-1}P^{ij}][(P^j)^{-1} - K] \\ &\quad \cdot [(G^i)' - (P^i)^{-1}P^{ij}]' \\ &\triangleq (P^i)^{-1} + (G^i)'(P^j)^{-1}G^i - K_c \\ &= J(P^{ij} = 0) - K_c \end{aligned} \tag{28}$$

where I is the identity matrix and

$$K \triangleq (P^j)^{-1}W(P^j)^{-1}[I + W(P^j)^{-1}]^{-1} \tag{29}$$

$$\begin{aligned} K_c &\triangleq [(G^i)' - (P^i)^{-1}P^{ij}]K[(G^i)' - (P^i)^{-1}P^{ij}]' \\ &\quad + (P^i)^{-1}P^{ij}(P^j)^{-1}G^i + [(P^i)^{-1}P^{ij}(P^j)^{-1}(G^i)]' \\ &\quad - [(P^i)^{-1}P^{ij}](P^j)^{-1}[(P^i)^{-1}P^{ij}]'. \end{aligned} \tag{30}$$

Setting $P^{ij} = 0$ and $P^{ij} \neq 0$ for the estimation from the heterogenous local sensors correspond to "uncorr" and "corr" assumptions, respectively. For the homogeneous case, the crosscovariance matrix is always positive; this follows from the Lyapunov equation (9.3.2–3) in [3]. However, in the heterogeneous (and nonlinear) case, K_c may be indefinite (some eigenvalues are positive and some negative). Therefore, accounting for it (as opposed to assuming it zero) yields the exact (optimal) variance larger in some state components and smaller in others.

The results using a simple functional model of the crosscorrelation of the estimation errors ($\tilde{\mathbf{x}}^i$ and $\tilde{\mathbf{x}}^j$), based on the polar-to-Cartesian transformation, are shown in Appendix D and they do not provide any perceivable benefits. As discussed above, for the linear-Gaussian and symmetric case, neglecting the common process noise makes the fusion optimistic. For the nonlinear case examined, neglecting it makes the fusion sometimes optimistic and sometimes pessimistic, but the effect is small. This supports the approach of ignoring the dependency between the tracks from different local sensors.[5] Thus, since the maneuvers are unknown and scenario dependent, we pursue the heterogeneous T2TF without considering the crosscorrelation between the estimation errors.

5. SIMULATION RESULTS

A typical two-dimensional scenario for heterogenous T2TF is with an active sensor located at (x_a, y_a), with measurements of target range and azimuth angle

$$r = \sqrt{(x - x_a)^2 + (y - y_a)^2} + w_r \tag{31}$$

$$\theta_a = \tan^{-1}\left(\frac{y - y_a}{x - x_a}\right) + w_a \tag{32}$$

and a passive sensor located at (x_p, y_p), with the azimuth angle measurements

$$\theta_p = \tan^{-1}\left(\frac{y - y_p}{x - x_p}\right) + w_p \tag{33}$$

where w_r, w_a and w_p are mutually independent zero mean white Gaussian noises with standard deviations (SD) σ_r, σ_a and σ_p, respectively.

The ground truth is a target moving with a constant speed of 250 m/s with initial state in Cartesian coordinates (with position in m)

$$\begin{aligned} \mathbf{x}^i(0) &= [x(0) \quad \dot{x}(0) \quad y(0) \quad \dot{y}(0)]' \\ &= [0 \quad 0 \quad 20000 \quad 250]'. \end{aligned} \tag{34}$$

At $t = 100$ s it starts a left turn of 2°/s (about 30 mrad/s) for 30 s, then continues straight until $t = 200$ s, at which time it turns right with 1°/s for 45 s, then left with 1°/s for 90 s, then right with 1°/s for 45 s, then continues straight until 50 s.

The measurements of the active sensor located at $(-6 \cdot 10^4, 2 \cdot 10^4)$ m are made every $T_a = 5$ s, starting from $k = 0$ with measurement noise SD as $\sigma_r = 20$ m and $\sigma_a = 5$ mrad. An unbiased measurement conversion from polar coordinates to Cartesian coordinates (denoted as $\mathbf{z}^i$ with $\mathbf{w}^i$ for polar coordinates and $\mathbf{z}_c^i$ with $\mathbf{w}_c^i$ for Cartesian coordinates, respectively) is done for the active sensor measurements for filtering [2]. The measurements of the passive sensor located at $(-5 \cdot 10^4, 4 \cdot 10^4)$ m are made every $T_p = 1$ s, starting from $k = 0$ with measurement noise $\sigma_p = 1$ mrad. This scenario is shown in Fig. 1.

The active sensor uses an interacting multiple model (IMM) estimator using continuous time white noise

[5] We are grateful for the anonymous reviewer who summarized so well our findings.

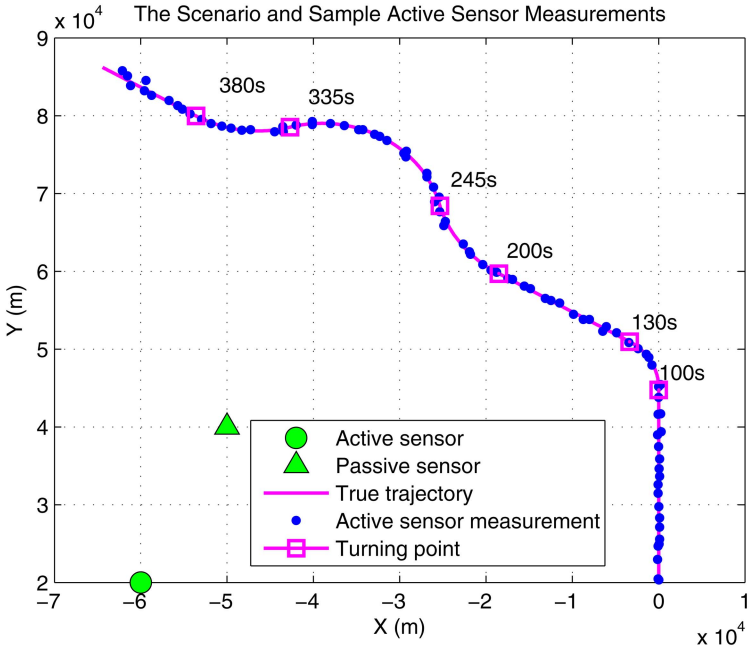

Fig. 1. The scenario.

acceleration (CWNA) model [2]. The passive sensor uses, for reasons shown in Appendix E, a linear Kalman filter (KF) using a continuous time Wiener process acceleration (CWPA) model [2].

5.1. The Active Sensor IMM Estimator Design

For the active sensor IMM, in order to cover the uniform motion segments and maneuvering segments in the trajectory, two modes are used: one mode using a linear nearly constant velocity (NCV) model that includes 4 state components (the Cartesian position and velocity in X- and Y-coordinates) and the other mode using a nearly coordinated turn (NCT) model that includes that 5 state components (the Cartesian position and velocity in X- and Y-coordinates and the turn rate Ω)

$$\begin{aligned}\mathbf{x}_a^i(k) &\triangleq [x(k) \quad \dot{x}(k) \quad y(k) \quad \dot{y}(k) \quad \Omega(k)]' \\ &= [\mathbf{x}^i(k)' \quad \Omega(k)]'. \end{aligned} \tag{35}$$

Since the conventional mixing [2] in an IMM estimator with modes that have unequal dimension state vectors will lead to bias in the estimates of the non-common state component(s), the unbiased mixing approach described in [13] is used to overcome this bias problem (for the turn rate in this case).

The NCV model for uniform motion segment is implemented as the following discretized CWNA model [2] (with low-level process noise)

$$\mathbf{x}^i(k+1) = F^i(k)\mathbf{x}^i(k) + \mathbf{v}^i(k) \tag{36}$$

$$\mathbf{z}_c^i(k) = H^i(k)\mathbf{x}^i(k) + \mathbf{w}_c^i(k) \tag{37}$$

where, with T_a is the sampling interval of the active sensor,[6]

$$F^i = \begin{bmatrix} 1 & T_a & 0 & 0 \\ 0 & 1 & 0 & 0 \\ 0 & 0 & 1 & T_a \\ 0 & 0 & 0 & 1 \end{bmatrix} \tag{38}$$

$$H^i = \begin{bmatrix} 1 & 0 & 0 & 0 \\ 0 & 0 & 1 & 0 \end{bmatrix} \tag{39}$$

and the covariance matrix of the process noise $\mathbf{v}^i(k)$ is

$$\begin{aligned} Q^i(k) &\triangleq E[\mathbf{v}^i(k)\mathbf{v}^i(k)'] \\ &= \begin{bmatrix} \begin{bmatrix} \frac{T_a^3}{3} & \frac{T_a^2}{2} \\ \frac{T_a^2}{2} & T_a \end{bmatrix} q_a & \mathbf{0}_{2\times 2} \\ \mathbf{0}_{2\times 2} & \begin{bmatrix} \frac{T_a^3}{3} & \frac{T_a^2}{2} \\ \frac{T_a^2}{2} & T_a \end{bmatrix} q_a \end{bmatrix} \end{aligned} \tag{40}$$

where the continuous time process noise "intensities" q_a is the power spectral density (PSD). Note that the process noise induced root mean square (RMS) change in the velocity over a sampling interval T_a is

$$d_a \triangleq \frac{\sqrt{q_a T_a}}{T_a} \tag{41}$$

whose physical dimensions is linear acceleration [12].

[6] Different sampling rates may be possible and T_a is replaced by the time-variant $T_a(k) \triangleq t(k+1) - t(k)$.

The NCT model, commonly refers to a target maneuver executed under nearly constant speed along a nearly circular path, is implemented as the following discretized continuous-time coordinated turn dynamic model [8]

$$\mathbf{x}_a^i(k+1) = f_a^i[\mathbf{x}_a^i(k)] + \mathbf{v}_a^i[\mathbf{x}_a^i(k)] \tag{42}$$

$$\mathbf{z}_c^i(k) = H_a^i \mathbf{x}_a^i(k) + \mathbf{w}_c^i(k) \tag{43}$$

where

$$f_a^i[\mathbf{x}_a^i(k)] = \begin{bmatrix} x(k) + T_a\dot{x}(k) - T_a^2\Omega(k)\dot{y}(k)/2 \\ \dot{x}(k) - T_a\Omega(k)\dot{y}(k) - T_a^2\Omega(k)^2\dot{x}(k)/2 \\ y(k) + T_a\dot{y}(k) + T_a^2\Omega(k)\dot{x}(k)/2 \\ \dot{y}(k) + T_a\Omega(k)\dot{x}(k) - T_a^2\Omega(k)^2\dot{y}(k)/2 \\ \Omega(k) \end{bmatrix} \tag{44}$$

$$H_a^i = \begin{bmatrix} 1 & 0 & 0 & 0 & 0 \\ 0 & 0 & 1 & 0 & 0 \end{bmatrix} \tag{45}$$

and the process noise for the NCT model depends on current target state (target velocity components and turn rate). The covariance matrix of the target state-dependent process noise $\mathbf{v}_a^i[\mathbf{x}_a^i(k)]$ can be roughly shown as (the detailed form can be found in Appendix B)[7]

$$Q_a^i[\mathbf{x}_a^i(k)] \triangleq E\{\mathbf{v}_a^i[\mathbf{x}_a^i(k)]\mathbf{v}_a^i[\mathbf{x}_a^i(k)]'\} = \begin{bmatrix} \frac{T_a^3}{3}\frac{\dot{x}(k)^2}{\dot{x}(k)^2+\dot{y}(k)^2}q_a & \times & \times & \times & \times \\ \times & \times & \times & \times & \times \\ \times & \times & \frac{T_a^3}{3}\frac{\dot{y}(k)^2}{\dot{x}(k)^2+\dot{y}(k)^2}q_a & \times & \times \\ \times & \times & \times & \times & \times \\ \times & \times & \times & \times & Tq_\Omega \end{bmatrix} \tag{46}$$

where the continuous time process noise "intensities" q_a and q_Ω are the PSDs.

Note that the process noise induced RMS change over a sampling interval T_a in the velocity is as in (41) and in the turn rate is

$$d_\Omega \triangleq \frac{\sqrt{q_\Omega T_a}}{T_a} \tag{47}$$

whose physical dimensions is turn acceleration [12]. The d_a and d_Ω are the design values used to select the process noise PSDs. A guideline for the choice of these process noise intensities for the NCT model is shown in Appendix B.

As the NCT model described in (42) is nonlinear, extended KF (EKF) has been used as the mode-matched filter for the NCT model in active sensor IMM. We only use the estimate $\hat{\mathbf{x}}^i(k)$ (from $\hat{\mathbf{x}}_a^i(k)$) and the corresponding covariance matrix $P^i(k)$ for the fusion.

TABLE I
The RMS Change Rate Due to Process Noise

	d_a (m/s^2)	d_Ω (mrad/s^2)
Mode 1 (NCV)	0.2	N/A
Mode 2 (NCT)	1	2

For the active sensor IMM estimator with unbiased converted measurements (in Cartesian coordinates), the process noises design values are summarized in Table I and the corresponding transition probability matrix is (based on the mean sojourn time [2])

$$\pi_{CT} = \begin{bmatrix} 0.9 & 0.1 \\ 0.1 & 0.9 \end{bmatrix} \tag{48}$$

with initial mode probability vector $[0.9, 0.1]$.

5.2 The Passive Sensor KF Estimator Design

For the passive sensor, as pointed out in Appendix C, the target maneuvering index is very small and the target maneuvers are nearly unobservable by the passive sensor. Consequently, a single model filter (i.e., a linear KF) has been chosen as the local estimator, with the state vector

$$\mathbf{x}_p^j \triangleq [\theta \quad \dot{\theta} \quad \ddot{\theta}]' = [\mathbf{x}^j(k)' \quad \ddot{\theta}]'. \tag{49}$$

The discretized CWPA model [2] in the angle, angle rate and angle acceleration space is

$$\mathbf{x}_p^j(k+1) = F_p^j \mathbf{x}_p^j(k) + \mathbf{v}_p^j(k) \tag{50}$$

$$\mathbf{z}_p^j(k) = H_p^j \mathbf{x}_p^j(k) + \mathbf{w}_p^j(k) \tag{51}$$

where, with T_p the sampling interval of the passive sensor, we have

$$F_p^j = \begin{bmatrix} 1 & T_p & \frac{T_p^2}{2} \\ 0 & 1 & T_p \\ 0 & 0 & 1 \end{bmatrix} \tag{52}$$

$$H_p^j = [1 \quad 0 \quad 0] \tag{53}$$

[7]This "target state-dependent" process noise covariance matrix from [8] yielded superior RMSE performance (but no major change in the consistency) compared with the simplified covariance matrix from [2], Sec. 11.7.

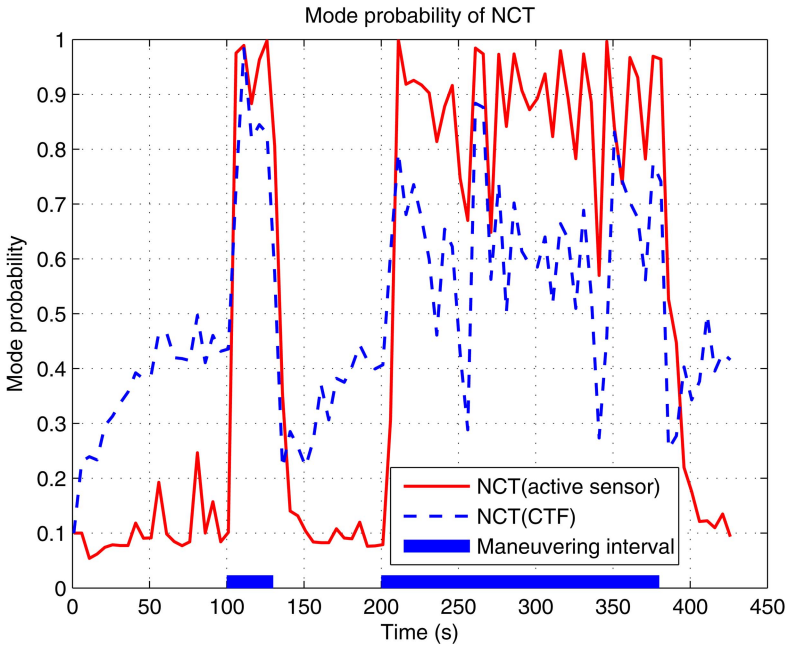

Fig. 2. The maneuvering mode probability (NCT) in the active sensor IMM and CTF IMM.

and the covariance matrix of the process noise is

$$Q_p^j(k) \triangleq E[\mathbf{v}_p^j(k)\mathbf{v}_p^j(k)'] = \begin{bmatrix} \frac{T_p^5}{20} & \frac{T_p^4}{8} & \frac{T_p^3}{6} \\ \frac{T_p^4}{8} & \frac{T_p^3}{3} & \frac{T_p^2}{2} \\ \frac{T_p^3}{6} & \frac{T_p^2}{2} & T_p \end{bmatrix} q_p. \tag{54}$$

Note that for the PSD q_p, the process noise induced RMS change in the angular acceleration over T_p is

$$d_p \triangleq \frac{\sqrt{q_p T_p}}{T_p} \tag{55}$$

whose physical dimension is angular jerk (derivative of acceleration).

The process noise design value chosen for the passive sensor is $d_p = 0.04$ (mrad/s^3). We only use the estimate $\hat{\mathbf{x}}^j(k)$ (from $\hat{\mathbf{x}}_p^j(k)$) and the corresponding covariance matrix $P^j(k)$ for the fusion.

5.3. The Heterogeneous T2TF

The LMMSE and ML heterogeneous T2TF are carried out at the FC every $T_f = 5$ s under the "uncorr" assumption, with the local estimates $\hat{\mathbf{x}}^i(k)$ (from $\hat{\mathbf{x}}_a^i(k)$) and $\hat{\mathbf{x}}^j(k)$ (from $\hat{\mathbf{x}}_p^j(k)$) and their corresponding covariance matrices $P^i(k)$ and $P^j(k)$. The CTF uses the same IMM design (CTF IMM for short) as the active sensor IMM estimator. The FC can run the fusion at an arbitrarily low rate or "on demand."

1) *The LMMSE Fuser*: In Figs. 3 and 4, the root mean square errors (RMSE) for the LMMSE fuser (with $T_f = 5$ s under the "uncorr" assumption) are compared with those for the active sensor's IMM estimator and the CTF IMM in position and velocity, respectively. It can be seen that the LMMSE heterogeneous T2TF approach always provides significantly better estimation performance than the single (active) sensor case.

The LMMSE heterogeneous T2TF provides larger RMSE than the CTF IMM in the non-maneuvering intervals but smaller RMSE if there is a maneuver. This degradation of the CTF in both position and velocity during the maneuvering intervals is because the CTF is using an IMM estimator, which is inappropriate for the passive sensor (due to the very small maneuver index). While using the IMM estimator is generally beneficial for maneuvering targets, the use of an IMM estimator with a sensor that cannot "see" the maneuvers can lead to performance degradation (the CTF IMM's performance at some fusion points is even worse than the active sensor IMM's). As shown in Appendix E, the maneuvering index from the passive sensor's view is so small that when the passive sensor measurements (with higher sampling rate than those of the active sensor) are sent to FC and processed centrally, these measurements increase the uncertainty about the target maneuvers.

From the maneuvering mode probability (NCT) in the active sensor IMM and in the CTF IMM, shown in Fig. 2, it can be seen that the CTF IMM cannot "see" the maneuvers at the times when there is only a passive sensor measurement and its maneuvering mode probability becomes too small. The use of the passive measurements in the CTF IMM "clouds" the maneuvers—it is preferable to have an active sensor IMM (which does detect the maneuvers) and a passive sensor KF (since the passive sensor is almost "blind" to the maneuvers) and fuse the outputs of these two local trackers.

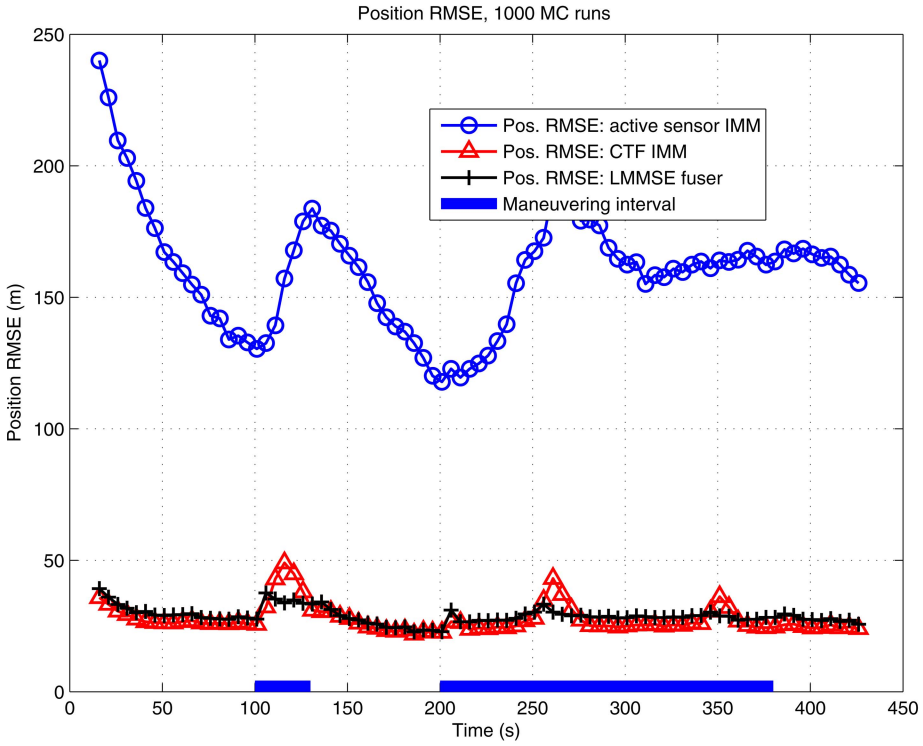

Fig. 3. The position RMSE for LMMSE fuser.

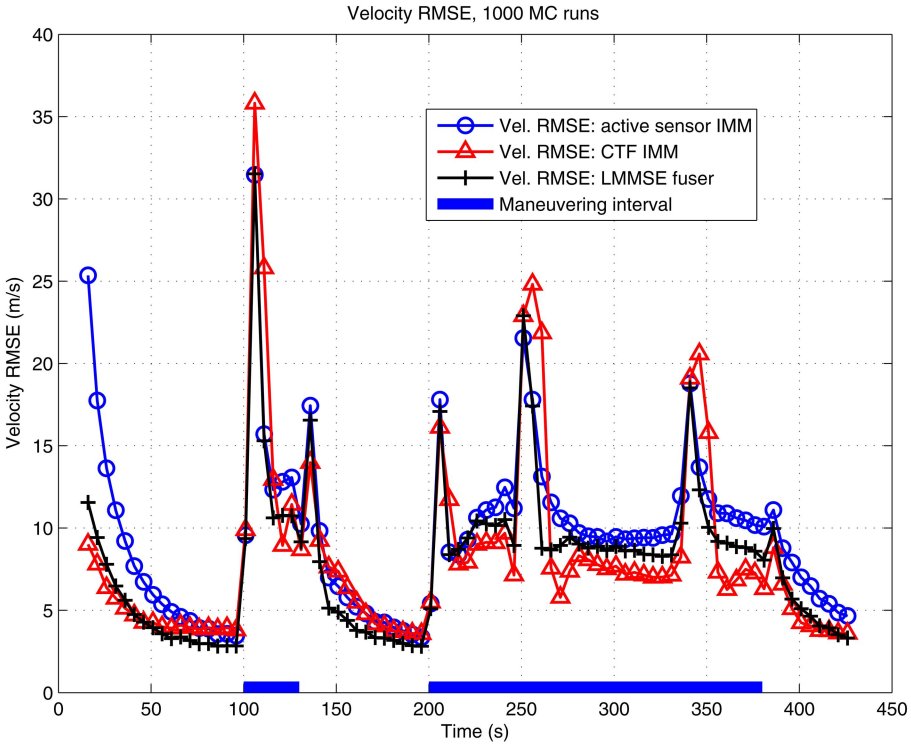

Fig. 4. The velocity RMSE for LMMSE fuser.

The observation from Figs. 3 and 4 that the CTF IMM performs during target maneuvers worse than the heterogeneous T2TF points out that the heterogeneous T2TF benefits from the freedom of having more suitable filters for the individual local sensors. This freedom can provide final fusion results comparable or even better than the corresponding CTF estimator.

We evaluate the fusion consistency of the LMMSE fuser by the normalized estimation error square (NEES) consistency test [2]. The NEES for the LMMSE fusion approach are shown in Fig. 5. The reason for the inconsistency of the fused estimates are (i) the local IMM estimator (for the active sensor) and the KF estimator (for the passive sensor) are not entirely

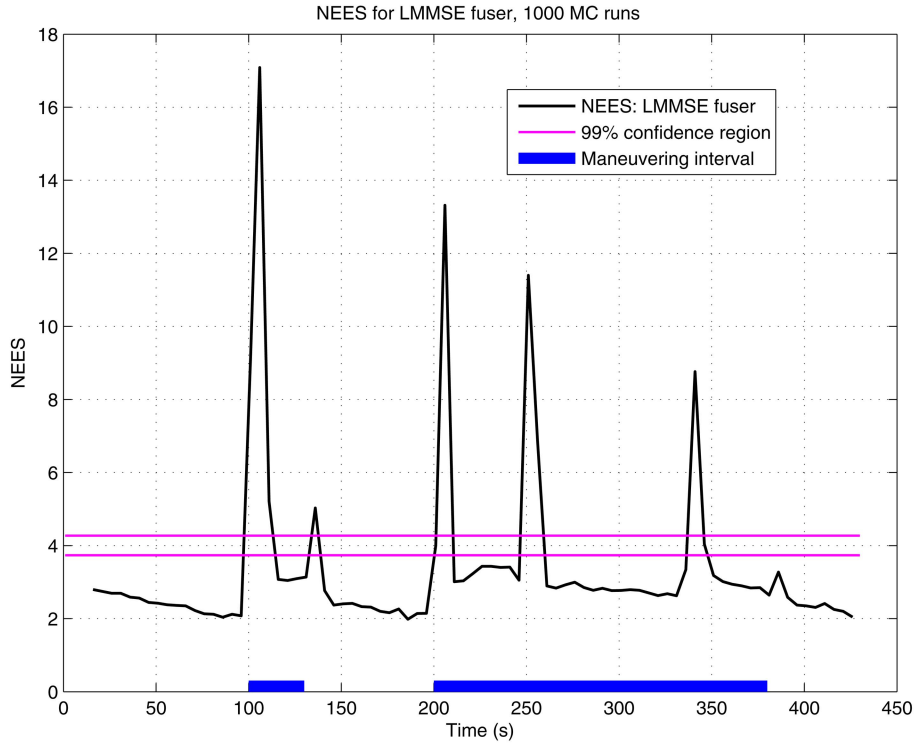

Fig. 5. The NEES for LMMSE fuser.

consistent[8] (as shown in Appendix F) and (ii) the cross-covariance has been assumed zero. Nevertheless, the quality of the estimates is improved by fusion, which justifies the approach. At this point, there is no known way to improve the sometimes optimistic, sometimes pessimistic behavior of the IMM—it is the inconsistency that drives its adaptation.

2) *The ML Fuser*: Using a numerical search (the gradient projection algorithm), the RMSE in position and velocity for the ML fuser are shown (with T_f = 5 s under the "uncorr" assumption) in Fig. 6 and Fig. 7, respectively. It can be seen that both the LMMSE fuser and the ML fuser give practically the same RMSE in position and velocity and both have better performances than the single (active) sensor case. As pointed out in [4], the LMMSE fuser is, in the linear-Gaussian case, actually optimal in the ML sense. Since the ML fuser in the heterogenous case (with nonlinearity) needs to be implemented by a time-consuming numerical search, the LMMSE fuser can be considered as an efficient and effective alternative for the ML fuser.

6. CONCLUSIONS

Examining the differences between the heterogeneous and homogeneous T2TF, this paper investigates the major difficulties of heterogenous T2TF. The LMMSE and the ML approaches for heterogenous T2TF are presented and compared with the corresponding CTF. The simulation study shows that both approaches can effectively achieve improved performance over the single sensor track quality and comparable performance to the CTF track. The use of the passive measurements in the CTF IMM "clouds" the maneuvers—it is preferable to have an active sensor IMM (which does detect the maneuvers) and a passive sensor KF (since the passive sensor is almost "blind" to the maneuvers) and fuse the outputs of these two local trackers. The freedom available to each local sensor to flexibly design a more suitable local estimator allows the heterogeneous T2TF approach to achieve a better estimation performance than the CTF IMM in the scenario considered. As the LMMSE T2TF has practically the same performance as the ML T2TF, it can be considered as an effective and efficient alternative for the numerical search required by the ML approach. The estimation errors' crosscorrelation has been examined by MC simulations. As it is impossible to predict maneuvers in a trajectory and there is no known way to correctly quantify the crosscorrelation of the estimation errors from heterogeneous local sensors, the heterogeneous T2TF was carried out assuming the tracks from the heterogeneous local sensors as uncorrelated.

[8]The IMM estimator is the worst estimator in terms of consistency except for all the other estimators [3]. However, it is the "short term" inconsistency that is the key for the capability of the IMM estimator to adapt itself to the observed behavior of the target (large innovations).

APPENDIX A. TAYLOR SERIES APPROXIMATION FOR THE LMMSE FUSER

By the first order Taylor expansion, we have

$$g(\mathbf{x}^i) \approx g(\hat{\mathbf{x}}^i) + G^i(\mathbf{x}^i - \hat{\mathbf{x}}^i) \tag{56}$$

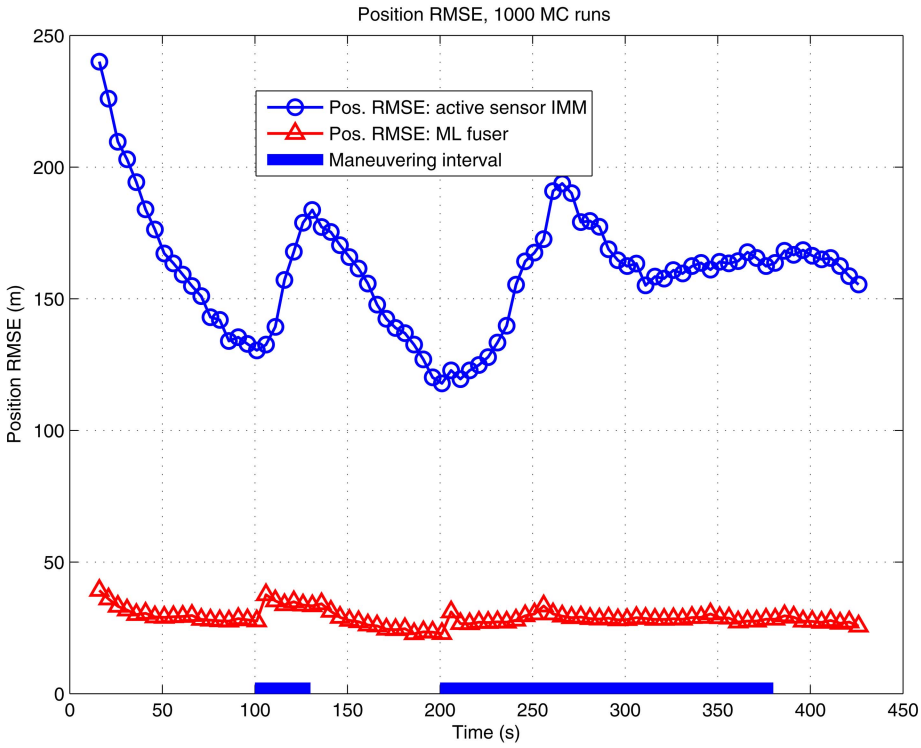

Fig. 6. The position RMSE for ML fuser.

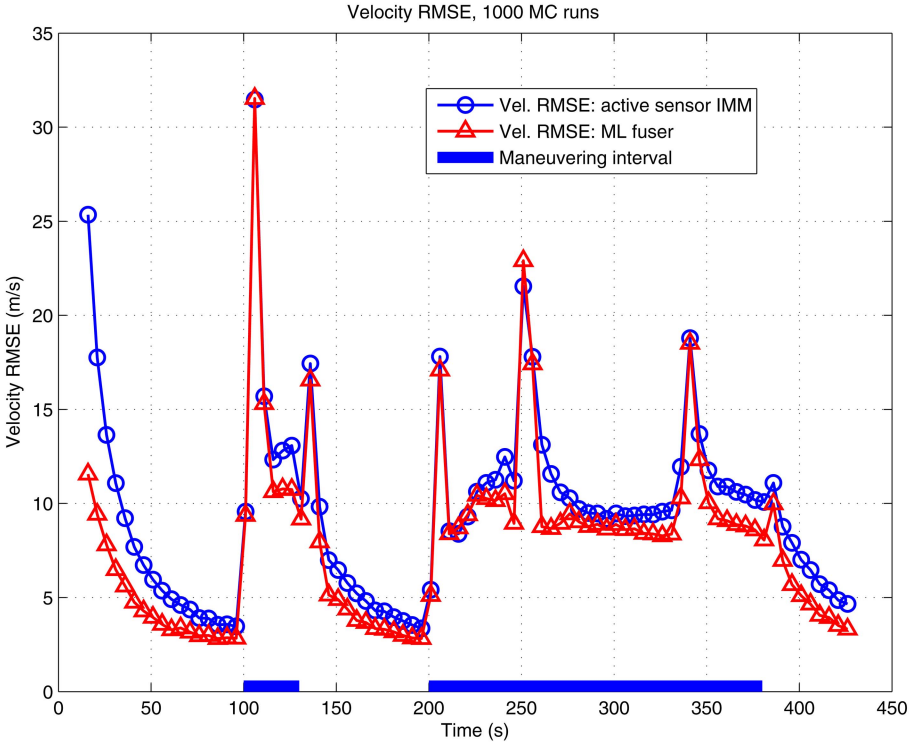

Fig. 7. The velocity RMSE for ML fuser.

where G^i is the Jacobian of $g(\mathbf{x}^i)$ evaluated at $\hat{\mathbf{x}}^i$, as defined in (17). Then (with the knowledge that $\mathbf{x}^j = g(\mathbf{x}^i)$)

$$\begin{aligned}\hat{\mathbf{x}}^j - g(\hat{\mathbf{x}}^i) &= \hat{\mathbf{x}}^j - g(\mathbf{x}^i) + G^i(\mathbf{x}^i - \hat{\mathbf{x}}^i) \\ &= G^i(\mathbf{x}^i - \hat{\mathbf{x}}^i) - (\mathbf{x}^j - \hat{\mathbf{x}}^j). \end{aligned} \tag{57}$$

So

$$\begin{aligned} P_{\mathbf{xz}} &\triangleq E[(\mathbf{x}^i - \hat{\mathbf{x}}^i)(\hat{\mathbf{x}}^j - g(\hat{\mathbf{x}}^i))'] \\ &\approx E[(\mathbf{x}^i - \hat{\mathbf{x}}^i)(G^i(\mathbf{x}^i - \hat{\mathbf{x}}^i) - (\mathbf{x}^j - \hat{\mathbf{x}}^j))'] \\ &= E[(\mathbf{x}^i - \hat{\mathbf{x}}^i)(\mathbf{x}^i - \hat{\mathbf{x}}^i)'](G^i)' - E[(\mathbf{x}^i - \hat{\mathbf{x}}^i)(\mathbf{x}^j - \hat{\mathbf{x}}^j)'] \\ &= P^i(G^i)' - P^{ij} \end{aligned} \tag{58}$$

and

$$P_{\mathbf{zz}} \triangleq E[(\hat{\mathbf{x}}^j - g(\hat{\mathbf{x}}^i))(\hat{\mathbf{x}}^j - g(\hat{\mathbf{x}}^i))']$$

$$\approx E[(G^i(\mathbf{x}^i - \hat{\mathbf{x}}^i) - (\mathbf{x}^j - \hat{\mathbf{x}}^j))(G^i(\mathbf{x}^i - \hat{\mathbf{x}}^i) - (\mathbf{x}^j - \hat{\mathbf{x}}^j))']$$

$$= P^j - G^i P^{ij} - P^{ji}(G^i)' + G^i P^i (G^i)'. \quad (59)$$

APPENDIX B. THE TARGET STATE-DEPENDENT PROCESS NOISE COVARIANCE MATRIX FOR THE NCT MODEL

As shown in [8], the target state-dependent process noise (in the Cartesian velocity model) is

$$\mathbf{v}_a^i[\mathbf{x}_a^i(k)] = D_a^i[\mathbf{x}_a^i(k)]\mathbf{v}_c^i(k) \quad (60)$$

where $\mathbf{v}_c^i(k) \sim \mathcal{N}(0, I_4)$ and

$$D_a^i[\mathbf{x}_a^i(k)] = S_a^i[\mathbf{x}_a^i(k)]V_a^i(k) \quad (61)$$

with

$$S_a^i[\mathbf{x}_a^i(k)] = \begin{bmatrix} \sqrt{q_a}s_1(k) & 0 & 0 & 0 \\ 0 & \sqrt{q_a}s_3(k) & -\sqrt{q_\Omega}\dot{y}(k) & 0 \\ \sqrt{q_\Omega}s_2(k) & 0 & 0 & 0 \\ 0 & \sqrt{q_a}s_4(k) & \sqrt{q_\Omega}\dot{x}(k) & 0 \\ 0 & 0 & 0 & \sqrt{q_\Omega} \end{bmatrix} \quad (62)$$

$$V_a^i(k) = \begin{bmatrix} \sqrt{T_a^3/3} & 0 & 0 & 0 \\ \frac{\sqrt{3T_a}}{2} & \frac{\sqrt{T_a}}{2} & 0 & 0 \\ 0 & 0 & \sqrt{T_a^3/3} & 0 \\ 0 & 0 & \frac{\sqrt{3T_a}}{2} & \frac{\sqrt{T_a}}{2} \end{bmatrix} \quad (63)$$

where q_a and q_Ω are the continuous-time process noise PSDs and

$$s_1(k) = \frac{\dot{x}(k)}{\sqrt{\dot{x}^2(k) + \dot{y}^2(k)}} \quad (64)$$

$$s_2(k) = \frac{\dot{y}(k)}{\sqrt{\dot{x}^2(k) + \dot{y}^2(k)}} \quad (65)$$

$$s_3(k) = \frac{\dot{x}(k) - T_a\Omega(k)\dot{y}(k)}{\sqrt{\dot{x}^2(k) + \dot{y}^2(k)}} \quad (66)$$

$$s_4(k) = \frac{\dot{y}(k) + T_a\Omega(k)\dot{x}(k)}{\sqrt{\dot{x}^2(k) + \dot{y}^2(k)}}. \quad (67)$$

We have the corresponding target state-dependent process noise covariance matrix (the time index k is ignored for conciseness)

$$Q_a^i[\mathbf{x}_a^i(k)] \triangleq E\{\mathbf{v}_a^i[\mathbf{x}_a^i(k)]\mathbf{v}_a^i[\mathbf{x}_a^i(k)]'\} \quad (68)$$

$$= E\{[D_a^i[\mathbf{x}_a^i(k)]\mathbf{v}_c^i(k)][D_a^i[\mathbf{x}_a^i(k)]\mathbf{v}_c^i(k)]'\} \quad (69)$$

$$= \begin{bmatrix} \frac{T_a^3}{3}s_1^2q_a & \frac{T_a^2}{2}s_1s_3q_a & \frac{T_a^3}{3}s_1s_2q_a & \frac{T_a^2}{2}s_1s_4q_a & 0 \\ \frac{T_a^2}{2}s_1s_3q_a & \frac{T_a^3}{3}\dot{y}^2q_\Omega + T_as_3^2q_a & \frac{T_a^2}{2}s_2s_3q_a & -\frac{T_a^3}{3}\dot{x}\dot{y}q_\Omega + T_as_3s_4q_a & -\frac{T_a^2}{2}\dot{y}q_\Omega \\ \frac{T_a^3}{3}s_1s_2q_a & \frac{T_a^2}{2}s_2s_3q_a & \frac{T_a^3}{3}s_2^2q_a & \frac{T_a^2}{2}s_2s_4q_a & 0 \\ \frac{T_a^2}{2}s_1s_4q_a & -\frac{T_a^3}{3}\dot{x}\dot{y}q_\Omega + T_as_3s_4q_a & \frac{T_a^2}{2}s_2s_4q_a & \frac{T_a^3}{3}\dot{x}^2q_\Omega + T_as_4^2q_a & \frac{T_a^2}{2}\dot{x}q_\Omega \\ 0 & -\frac{T_a^2}{2}\dot{y}q_\Omega & 0 & \frac{T_a^2}{2}\dot{x}q_\Omega & T_aq_\Omega \end{bmatrix}. \quad (70)$$

Guideline for Choice of Target State-Dependent Process Noise Intensity for the NCT Model

Observing the diagonal elements of $Q_a^i[\mathbf{x}_a^i(k)]$ in (71), the process noise induced RMS change rate in the velocity (X- and Y-coordinate) and in the turn rate over a sampling interval T_a are

$$d_a^x \triangleq \frac{\sqrt{\frac{T_a^3}{3}\dot{y}^2q_\Omega + T_as_3^2q_a}}{T_a} \quad (71)$$

$$d_a^y \triangleq \frac{\sqrt{\frac{T_a^3}{3}\dot{x}^2q_\Omega + T_as_4^2q_a}}{T_a} \quad (72)$$

$$d_\Omega \triangleq \frac{\sqrt{T_aq_\Omega}}{T_a} \quad (73)$$

respectively. It is obvious that the choices of the design values d_a (d_a^x and d_a^y) and d_Ω need to be considered simultaneously.

To make things simpler, we consider an extreme case with $\dot{x} = 0$ (similar case for $\dot{y} = 0$). Given a target with speed V_s (which is equal to the magnitude of $\dot{y}$ in this

extreme case), we have

$$s_1^* = 0 \tag{74}$$

$$s_2^* = 1 \tag{75}$$

$$s_3^* = -T_a\Omega(k) \tag{76}$$

$$s_4^* = 1. \tag{77}$$

This leads to

$$d_a^{x*} = \frac{\sqrt{\frac{T_a^3}{3}V_s^2 q_\Omega + T_a^3\Omega^2(k)q_a}}{T_a} \tag{78}$$

$$d_a^{y*} = \frac{\sqrt{T_a q_a}}{T_a}. \tag{79}$$

Since the assumption is $\dot{x} = 0$, the process noise induced RMS change in X-coordinate velocity should be more sensitive compared with that in Y-coordinate. Given a conjectured choice as d_Ω and d_a, the process noise induced RMS change in X-coordinate velocity contributed by the PSD q_Ω and q_a are,

$$d_a^{x*}(q_\Omega, q_a = 0) = \frac{\sqrt{\frac{T_a^3}{3}V_s^2 q_\Omega}}{T_a} = \frac{T_a\dot{y}d_\Omega^*}{\sqrt{3}} \tag{80}$$

$$d_a^{x*}(q_\Omega = 0, q_a) = \frac{\sqrt{T_a^3\Omega^2(k)q_a}}{T_a} = \sqrt{T_a\Omega^2(k)q_a}. \tag{81}$$

It is important to compare those two values. The process noise induced RMS change rate for both the linear velocity and the turn rate should be within reasonable ranges over time interval T_a.

REMARKS

Without loss generality, based on (80), (81) and (82), the selections of the design values d_a and d_Ω for the NCT model are shown as (sequentially)

i) Select d_Ω, then $d_a^{x*}(q_\Omega, q_a = 0)$ has been obtained and should be in a reasonable range.

ii) Select d_a, then $d_a^{x*}(q_\Omega = 0, q_a)$ has been obtained and should be in a reasonable range. Further, d_a^{x*} should be not too big and d_a^{y*} should be not too small.

APPENDIX C. THE MC RESULTS FOR THE SAMPLE CROSSCORRELATION

The *sample crosscorrelation coefficient* between the lth component of $\mathbf{x}^i$ and the hth component of $\mathbf{x}^j$ in M MC runs at a particular point in time (not indicated, for conciseness) is

$$\hat{\rho}^M_{\mathbf{x}_l^i\mathbf{x}_h^j} \triangleq \frac{\sum_{m=1}^M(\hat{\mathbf{x}}_{l,m}^i - \mathbf{x}_l^i)(\hat{\mathbf{x}}_{h,m}^j - \mathbf{x}_h^i)}{\sqrt{\left[\sum_{m=1}^M(\hat{\mathbf{x}}_{l,m}^i - \mathbf{x}_l^i)^2\right]\left[\sum_{m=1}^M(\hat{\mathbf{x}}_{h,m}^j - \mathbf{x}_h^j)^2\right]}}. \tag{82}$$

The sample crosscorrelation coefficients of different heterogeneous components from 1000 MC runs, for the scenario described in Section 5, are shown in Figs. 8–11. It can be seen that the "common process noise effect," driven by real maneuvers here, leads to significant crosscorrelation between the estimation errors from the heterogeneous local sensors. Furthermore, both positive and negative crosscorrelations are observed. This motivates the geometry-based "functional model" discussed in Appendix D.

APPENDIX D. AN APPROXIMATION TECHNIQUE FOR THE CROSSCOVARIANCE MATRIX

By considering the steady-state case for a KF, an approximation technique for the evaluation of the crosscovariance matrix in the homogeneous case has been developed recently [5]. This technique, which relies on the crosscorrelation coefficients between the local estimates of the same state components, namely, position and velocity and the maneuvering indices at the different sensors, can be extended to heterogeneous case as follows.

The components of the state $\mathbf{x}^i$ are grouped by coordinates ($c = 1,2$) as follows

$$\mathbf{x}_1^i = [x \quad \dot{x}]' \tag{83}$$

$$\mathbf{x}_2^i = [y \quad \dot{y}]' \tag{84}$$

which can be "aligned" with those of $\mathbf{x}^j$ as it will be shown in the sequel. Then the first components of $\mathbf{x}_c^i$, $c = 1,2$ and $\mathbf{x}^j$ are position and the second components are velocity, albeit in different spaces. The covariance submatrix P_c^i, corresponding to estimate $\hat{\mathbf{x}}_c^i$, follows from the corresponding elements of P^i.

Extending the crosscovariance matrix approximation technique for the homogeneous case in [5] to the heterogeneous case, we can then approximately reconstruct the crosscovariance matrix elements using the following expression

$$P_{c,lh}^{ij} = a_{c,lh}^{ij}\rho_{c,lh}^{ij}\sqrt{P_c^i(l,l)P^j(h,h)}, \qquad c = 1,2, \quad l,h = 1,2 \tag{85}$$

where $c = 1,2$ correspond to the first and the second part of the state $\mathbf{x}^i$; $l,h = 1$ represent position and $l,h = 2$ represent velocity; $\rho_{c,lh}^{ij}$ is the *maximum crosscorrelation coefficient* of the estimation errors in $\mathbf{x}_{c,l}^i$ and $\mathbf{x}_h^j$ and $a_{c,lh}^{ij}$ is geometry-dependent *adjustment factor* in the crosscorrelation coefficient. This factor is discussed below.

The maximum crosscorrelation coefficients are denoted as ρ_{pp} for position-position, ρ_{pv} for position-velocity, ρ_{vp} for velocity-position and ρ_{vv} for velocity-

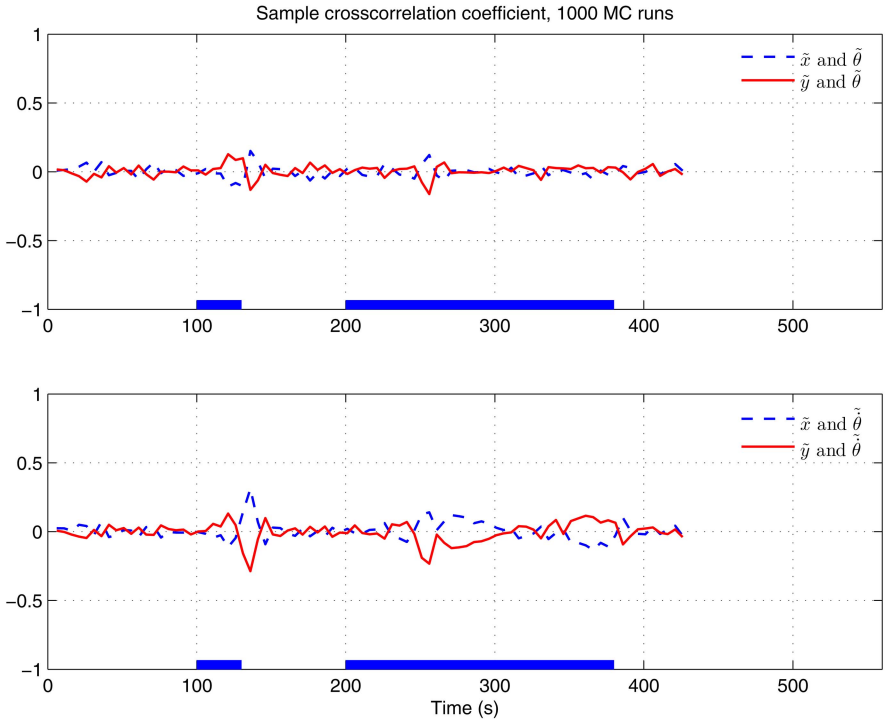

Fig. 8. The sample crosscorrelation for $\tilde{x}$ and $\tilde{y}$ with $\tilde{\theta}$ and $\dot{\tilde{\theta}}$.

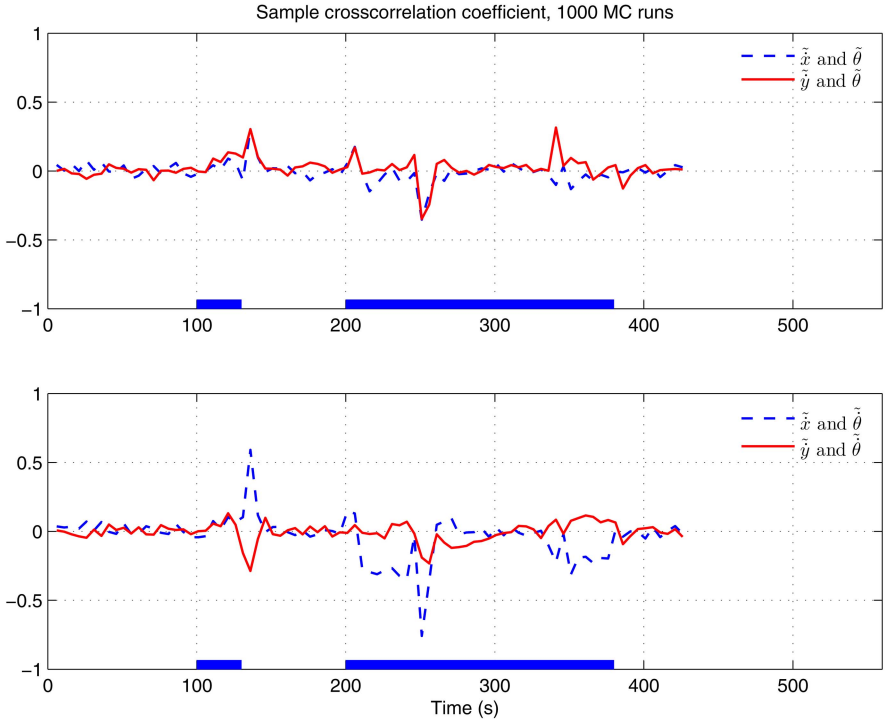

Fig. 9. The sample crosscorrelation for $\dot{\tilde{x}}$ and $\dot{\tilde{y}}$ with $\tilde{\theta}$ and $\dot{\tilde{\theta}}$.

velocity. Then we have

$$\rho_{c,lh}^{ij} = \begin{cases} \rho_{pp} & l,h = 1 \\ \rho_{pv} & l = 1, \quad h = 2 \\ \rho_{vp} & l = 2, \quad h = 1 \\ \rho_{vv} & l,h = 2 \end{cases} \tag{86}$$

which are chosen (similarly to [5]) as $\rho_{pp} = 0.1$, $\rho_{pv} = \rho_{vp} = 0.15$ and $\rho_{vv} = 0.45$ in our simulations.

There are two state variable pairs, say, x-θ and y-θ, for the position-position crosscorrelation coefficient. The best way to quantify the crosscorrelation difference (accounts for the geometry) for those state variable pairs is based on the function (7).

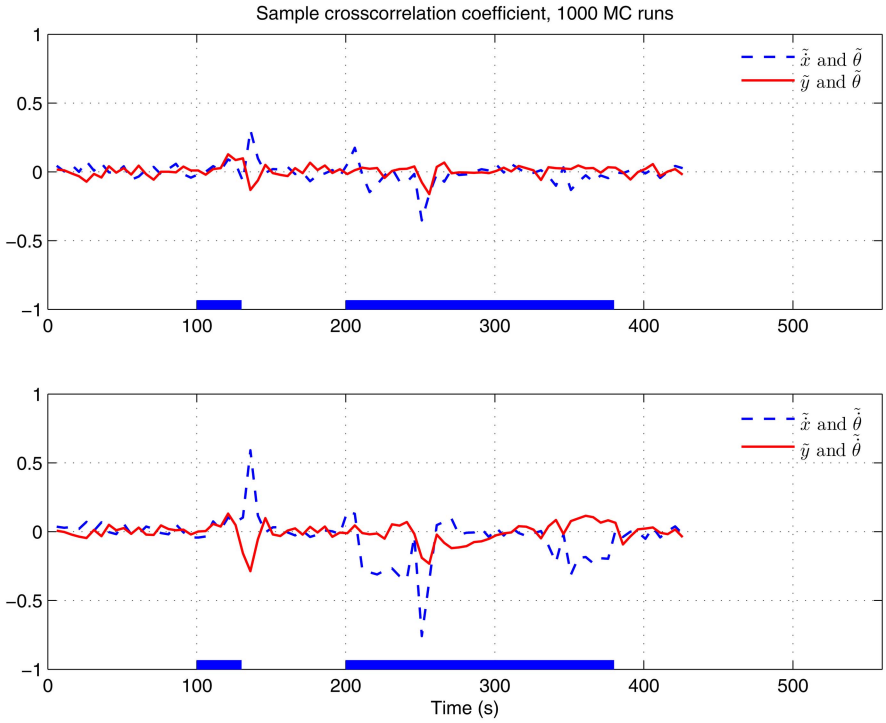

Fig. 10. The sample crosscorrelation for $\tilde{x}$ and $\tilde{y}$ with $\tilde{\theta}$ and $\dot{\tilde{\theta}}$.

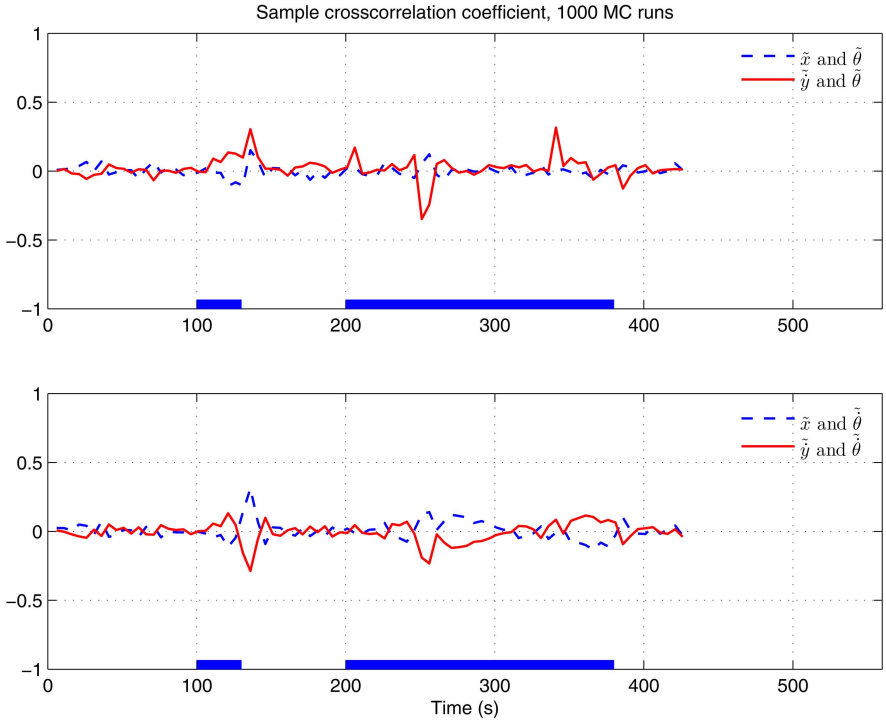

Fig. 11. The sample crosscorrelation for $\tilde{x}$ and $\dot{\tilde{y}}$ with $\tilde{\theta}$ and $\dot{\tilde{\theta}}$.

From the Cartesian to polar coordinate transformation (see, e.g., [4]), one has the following proportionalities

$$\frac{\partial x}{\partial \theta} \propto -\sin\theta \tag{87}$$

$$\frac{\partial y}{\partial \theta} \propto \cos\theta. \tag{88}$$

Based on the above, we have the following adjustment factors for the crosscorrelation coefficients of the pairs x-θ and y-θ

$$a^{ij}_{1,11} = -\sin\theta \tag{89}$$

$$a^{ij}_{2,11} = \cos\theta. \tag{90}$$

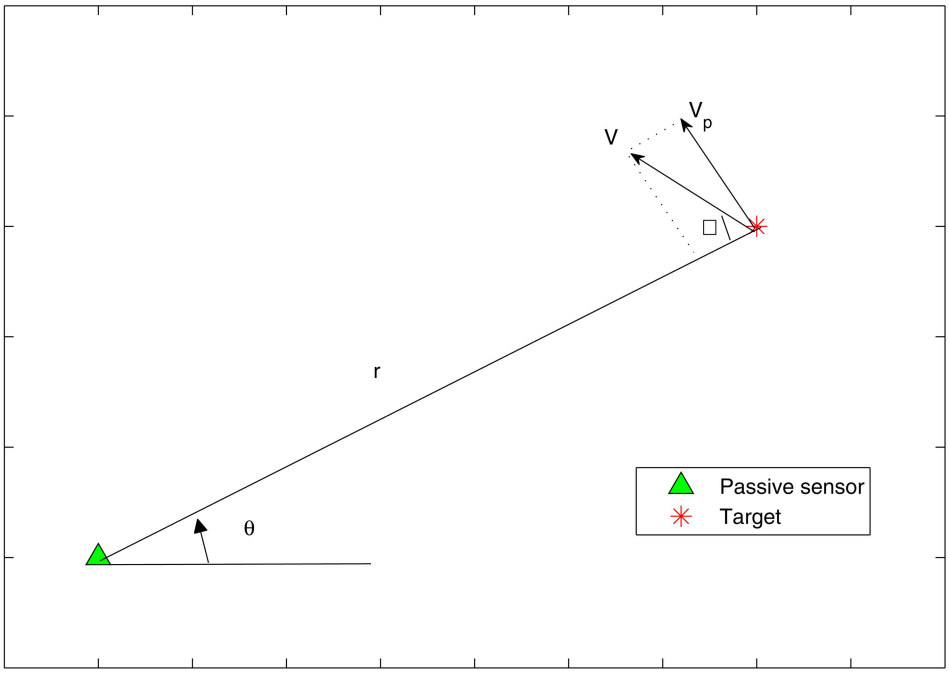

Fig. 12. The illustrated scenario for calculating target maneuvering index.

TABLE II
The RMSE in Position for LMMSE Fuser

	100 s	110 s	130 s	150 s	255 s
"uncorr"	27.6 m	37.5 m	33.6 m	28.9 m	30.3 m
"corr"	26.6 m	36.4 m	33.5 m	29.1 m	29.5 m

TABLE III
The RMSE in Velocity for LMMSE Fuser

	100 s	110 s	130 s	150 s	255 s
"uncorr"	9.4 m/s	15.3 m/s	10.7 m/s	5.1 m/s	17.4 m/s
"corr"	9.5 m/s	14.9 m/s	10.8 m/s	6.1 m/s	18.2 m/s

Then the crosscorrelation coefficients of the pairs x-θ and y-θ are obtained from combining the adjustment factor (90)–(91) with (87) as

$$\rho_{x\theta} = -\rho_{pp}\sin\theta \tag{91}$$

$$\rho_{y\theta} = \rho_{pp}\cos\theta. \tag{92}$$

Similarly, we have the adjustment factors

$$a_{c,lh}^{ij} = \begin{cases} -\sin(\theta), & c = 1 \\ \cos(\theta), & c = 2 \end{cases} \tag{93}$$

and the other crosscorrelation coefficients are

$$\rho_{x\dot{\theta}} = -\rho_{pv}\sin\theta \tag{94}$$

$$\rho_{y\dot{\theta}} = \rho_{pv}\cos\theta \tag{95}$$

$$\rho_{\dot{x}\theta} = -\rho_{vp}\sin\theta \tag{96}$$

$$\rho_{\dot{y}\theta} = \rho_{vp}\cos\theta \tag{97}$$

$$\rho_{\dot{x}\dot{\theta}} = -\rho_{vv}\sin\theta \tag{98}$$

$$\rho_{\dot{y}\dot{\theta}} = \rho_{vv}\cos\theta. \tag{99}$$

Finally, the reconstructed crosscovariance matrix is

$$P^{ij} = \begin{bmatrix} P_1^{ij} \\ P_2^{ij} \end{bmatrix} \tag{100}$$

with the elements of each block in (101) given by (86) with (88)–(100).

For the scenario described in Section 5, the RMSE in position and velocity under both "uncorr" and "corr" assumptions at some fusion times for the LMMSE fuser are shown in Table II and III, respectively.

Based on these results, which show negligible performance differences, it seems preferable to follow the "uncorr" assumption.

APPENDIX E. THE CHOICE OF ESTIMATOR FOR THE PASSIVE SENSOR

The guideline for deciding whether to use an IMM estimator or a (single model) KF can be quantified in terms of the target maneuvering index, which is the ratio between the standard deviation (RMS values) of the motion uncertainty and the measurement uncertainty [2][7]. Namely, if this index is below 0.5 then there is no point in using an IMM.

For the passive sensor considered, the maneuvering index can be calculated as follows. As shown in Fig. 12, the angular velocity seen by the passive sensor is

$$\dot{\theta}_p = \frac{V\sin\varphi}{r_p} \tag{101}$$

where V is the speed of the target and r_p is the range of the target from the passive sensor. Then the angular

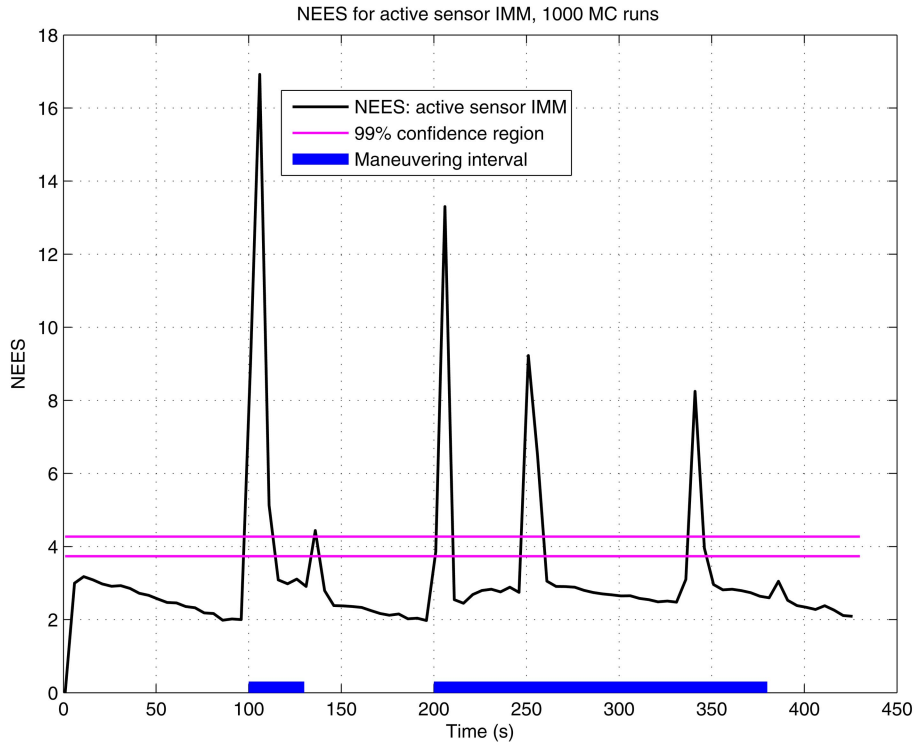

Fig. 13. The NEES for active sensor IMM.

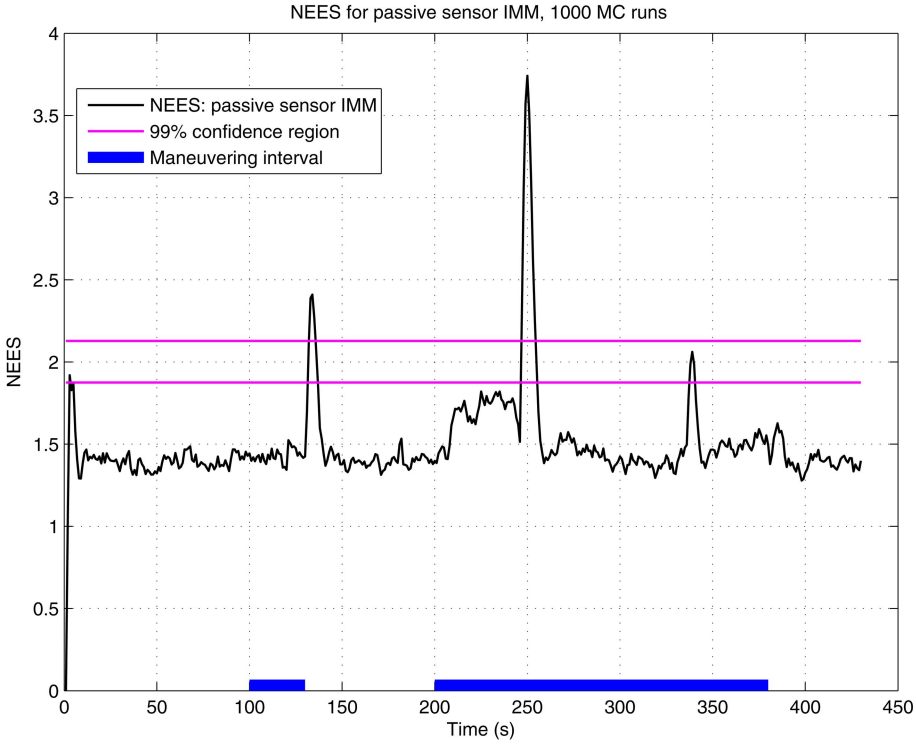

Fig. 14. The NEES for passive sensor KF.

acceleration seen by the passive sensor is

$$\ddot{\theta}_p = \frac{V\cos\varphi}{r_p}\dot{\varphi} \tag{102}$$

where $\dot{\varphi}$ is the target turn rate.

The RMS effect of (103) on the (angular) position, i.e., the angular displacement over sampling interval T_p (multiplied by 2) is $\ddot{\theta}_p T_p^2$. The (target's true) maneuvering index, with the passive sensor noise SD σ_p (in radians), is the (physically dimensionless)

quantity

$$\lambda_p = \frac{\ddot{\theta}_p T_p^2}{\sigma_p} = \frac{\dot{\varphi} T_p^2 V \cos\varphi}{\sigma_p r_p}. \quad (103)$$

For the scenario described in the simulation section, with $V = 250$ m/s, $\cos\varphi \approx 0.8$, $r_p \approx 5 \cdot 10^4$ m, $T_p = 1$ s, $\sigma_p = 1$ mrad and $\dot{\varphi} \approx 30$ mrad/s (which is the maximum target turn rate in our simulation scenario), we have $\lambda_p \approx 0.12$. This small target maneuvering index (less than 0.5) leads to the choice of a KF for the passive sensor, as done in Section 5.

APPENDIX F. THE LOCAL ESTIMATORS' CONSISTENCY

The NEES for the active sensor's IMM and for the passive sensor's KF are shown in Figs. 13 and 14 (the results are obtained by using the estimates and the corresponding covariance matrices for the heterogeneous T2TF, that is, four components' information from the active sensor and two components' information from the passive sensor), respectively. The lack of consistency of the passive sensor KF is due to the maneuvers. The lack of consistency of the active sensor IMM is common and this is due to its (unavoidable delay) in the adaptation. The IMM estimator is "pessimistic" during the no-maneuver intervals and "optimistic" when a maneuver starts or ends until it "catches up." This is the typical behavior of the IMM, which is still superior to any single-model based filter.

REFERENCES

[1] Y. Bar-Shalom and H. Chen
Covariance reconstruction for track fusion with legacy track sources.
Journal of Advances in Information Fusion, **3**, 2 (Dec. 2008), 107–117.

[2] Y. Bar-Shalom, X. R. Li, and T. Kirubarajan
Estimation with Applications to Tracking and Navigation: Algorithms and Software for Information Extraction.
Wiley, 2001.

[3] Y. Bar-Shalom, P. K. Willett, and X. Tian
Tracking and Data Fusion.
YBS Publishing, 2011.

[4] K. C. Chang, R. K. Saha, and Y. Bar-Shalom
On optimal track-to-track fusion.
IEEE Transactions on Aerospace and Electronic Systems, **33**, 4 (Oct. 1997), 1271–1276.

[5] H. Chen, T. Kirubarajan, and Y. Bar-Shalom
Performance limits of track-to-track fusion versus centralized estimation: Theory and application.
IEEE Transactions on Aerospace and Electronic Systems, **AES-39**, 2 (Apr. 2003), 386–398.

[6] H. Chen and Y. Bar-Shalom
Track association and fusion with heterogeneous local trackers.
Proceedings of 46th IEEE Conference on Decision and Control, New Orleans, LA, Dec. 2007.

[7] T. Kirubarajan and Y. Bar-Shalom
Kalman filter versus IMM estimator: When do we need the latter?
IEEE Transactions on Aerospace and Electronic Systems, **39**, 4 (Oct. 2003), 1452–1457.

[8] M. R. Morelande and N. J. Gordon
Target tracking through a coordinated turn.
Proceedings of IEEE International Conference on Acoustics, Speech, and Signal Processing (ICASSP '05), vol. 4, iv/21–iv/24, 2005.

[9] R. K. Saha
Track-to-track fusion with dissimilar sensors.
IEEE Transactions on Aerospace and Electronic Systems, **32**, 3 (July 1996), 1021–1029.

[10] X. Tian and Y. Bar-Shalom
Track-to-track fusion configurations and association in a sliding window.
Journal of Advances in Information Fusion, **4**, 2 (Dec. 2009), 146–164.

[11] X. Tian and Y. Bar-Shalom
The optimal algorithm for asynchronous track-to-track fusion.
Proceedings of SPIE Conference on Signal and Data Processing of Small Targets, #7698-46, Orlando, FL, Apr. 2010.

[12] T. Yuan, Y. Bar-Shalom, P. K. Willett, and D. Hardiman
Impact point prediction for short range thrusting projectiles.
Proceedings of SPIE Conference on Signal and Data Processing of Small Targets, #7698-55, Orlando, FL, Apr. 2010.

[13] T. Yuan, Y. Bar-Shalom, P. K. Willett, et. al
A multiple IMM approach with unbiased mixing for thrusting projectiles.
Submitted to *IEEE Transactions on Aerospace and Electronic Systems*.

Ting Yuan "TinYe" received B.S. and M.S. degrees both from the University of Electronic Science and Technology of China. He is currently pursuing the Ph.D. degree in electrical and computer engineering, University of Connecticut, Storrs.

His research interests include statistical signal processing and multisensor track/information fusion.

Yaakov Bar-Shalom (S'63—M'66—SM'80—F'84) was born on May 11, 1941. He received the B.S. and M.S. degrees from the Technion, Israel Institute of Technology, in 1963 and 1967 and the Ph.D. degree from Princeton University, Princeton, NJ, in 1970, all in electrical engineering.

From 1970 to 1976 he was with Systems Control, Inc., Palo Alto, CA. Currently he is Board of Trustees Distinguished Professor in the Department of Electrical and Computer Engineering and Marianne E. Klewin Professor in Engineering. He is also director of the ESP Lab (Estimation and Signal Processing) at the University of Connecticut. His research interests are in estimation theory and stochastic adaptive control and he has published over 360 papers and book chapters in these areas. In view of the causality principle between the given name of a person (in this case, "(he) will track," in the modern version of the original language of the Bible) and the profession of this person, his interests have focused on tracking.

He coauthored the monograph *Tracking and Data Association* (Academic Press, 1988), the graduate text *Estimation with Applications to Tracking and Navigation* (Wiley, 2001), the text *Multitarget-Multisensor Tracking: Principles and Techniques* (YBS Publishing, 1995), and edited the books *Multitarget-Multisensor Tracking: Applications and Advances* (Artech House, Vol. I 1990; Vol. II 1992, Vol. III 2000). He has been elected Fellow of IEEE for "contributions to the theory of stochastic systems and of multitarget tracking." He has been consulting to numerous companies, and originated the series of Multitarget Tracking and Multisensor Data Fusion short courses offered at Government Laboratories, private companies, and overseas.

During 1976 and 1977 he served as associate editor of the *IEEE Transactions on Automatic Control* and from 1978 to 1981 as associate editor of *Automatica*. He was program chairman of the 1982 American Control Conference, general chairman of the 1985 ACC, and cochairman of the 1989 IEEE International Conference on Control and Applications. During 1983–1987 he served as chairman of the Conference Activities Board of the IEEE Control Systems Society and during 1987–1989 was a member of the Board of Governors of the IEEE CSS. Currently he is a member of the Board of Directors of the International Society of Information Fusion and served as its Y2K and Y2K2 President. In 1987 he received the IEEE CSS distinguished Member Award. Since 1995 he is a distinguished lecturer of the IEEE AESS. He is corecipient of the M. Barry Carlton Awards for the best paper in the *IEEE Transactions on Aerospace and Electronic Systems* in 1995 and 2000, and received the 1998 University of Connecticut AAUP Excellence Award for Research, the 2002 J. Mignona Data Fusion Award from the DoD JDL Data Fusion Group, and the 2008 IEEE D. J. Picard Medal for Radar Technologies and Applications.

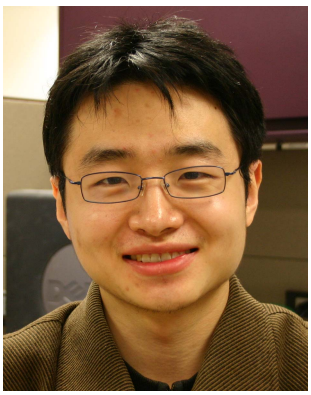

Xin Tian received the B.S. degree in 2002 and M.S. degree in 2005, both from the Department of Information and Communication Engineering, Xi'an Jiaotong University, China. In 2010 he received the Ph.D. degree from the Department of Electrical and Computer Engineering, University of Connecticut, Storrs.

Dr. Tian's research areas include statistical signal processing, tracking and information fusion algorithms, detection theory, decision theory under uncertainty, sensor management. He is currently a research scientist at I-fusion Inc., Germantown, MD.